Afyon Kocatepe Üniversitesi Fen ve Mühendislik Bilimleri Dergisi
Afyon Kocatepe University – Journal of Science and Engineering
https://dergipark.org.tr/tr/pub/akufemubid

Araştırma Makalesi / Research Article
e-ISSN: 2149-3367 DOI: https://doi.org/10.35414/akufemubid.1815973
CITE: Afyon Kocatepe University Journal of Science and Engineering 26(3) (2026) 583-592

Modulating Interfacial Charge Transfer in Dye-Sensitized Solar Cells with a Trimethoxy-Substituted Co-Adsorbent

*Makale Bilgisi / Article Info
Alındı/Received: 02.11.2025
Kabul/Accepted: 25.04.2026
Yayımlandı/Published: 03.06.2026

Trimetoksi Fonksiyonlu Bir Ko-adsorban ile Boya Duyarlı Güneş Hücrelerinde Arayüzey Yük Transferinin Ayarlanması

Adem MUTLU*

Ege University, Solar Energy Institute, İzmir, Türkiye

Abstract

Methoxy-substituted co-adsorbents offer a practical strategy to improve interfacial charge-transfer kinetics and reduce recombination losses in dye-sensitized solar cells (DSSCs). Here, a trimethoxy-substituted, *4-[5'-(3,4,5-trimethoxyphenyl)-2,2'-bithien-5-yl]benzoic acid*, (ZE-3MeO) is deployed as a co-adsorbent to regulate the TiO_2/N719/electrolyte interface. X-ray photoelectron spectroscopy (XPS) reveals an enhanced contribution of oxygenated-carbon signatures (C–O/C–O–C) consistent with an oxygen-enriched surface chemistry after adsorption. Electrochemical impedance spectroscopy (EIS) shows a pronounced reduction of the fitted high-frequency interfacial resistance (R_1=3.4 Ω, control: 6.7 Ω) and a markedly prolonged electron lifetime (τ_e=16.6 ms, control: 3.8 ms), consistent with mitigated interfacial recombination and improved charge-transfer/collection kinetics. Under AM1.5G illumination, the ZE-3MeO the best-performing device attains V_{oc}=680 mV, short circuit current density (J_{sc})=12.1 mA/cm^2, fill factor (FF)=61.5%, and photovoltaic conversion efficiency (PCE)=5.1% versus 4.1% for the unmodified control device, corresponding to a ~24% relative efficiency improvement and corroborated by incident photon-to-current efficiency (IPCE)-integrated photocurrents. Overall, these results show that trimethoxy-substituted co-adsorbents enhance passivation and interfacial charge transfer, providing design guidance for next-generation self-assembled monolayer (SAM)-like co-adsorbents in DSSCs.

Keywords: *Co-adsorbent; SAM; DSSCs; Solar cell; Interface modification; Efficiency*

Öz

Metoksi fonksiyonlu ko-adsorbanlar, boya duyarlı güneş hücrelerinde (DSSC'ler) arayüzey yük transfer kinetiğini iyileştirmek ve rekombinasyon kayıplarını azaltmak için pratik bir strateji sunmaktadır. Bu çalışmada, trimetoksi ile fonksiyonelleştirilmiş, *4-[5'-(3,4,5-trimetoksi fenil)-2,2'-bitien-5-il]benzoik asit* (ZE-3MeO), TiO_2/N719/elektrolit ara yüzeyini düzenlemek üzere ko-adsorban olarak kullanılmıştır. X-ışını fotoelektron spektroskopisi (XPS), adsorpsiyondan sonra oksijence zenginleşmiş yüzey kimyasıyla tutarlı olarak oksijenli karbon imzalarının (C–O/C–O–C) artan katkısını ortaya koymaktadır. Elektrokimyasal empedans spektroskopisi (EIS), yüksek frekansta arayüz direncinin (R_1=3,4 Ω, kontrol: 6,7 Ω) belirgin bir şekilde azaldığını ve elektron ömrünün (τ_e=16,6 ms, kontrol: 3,8 ms) önemli ölçüde uzadığını göstermektedir; bu da arayüz rekombinasyonunun azalması ve yük transferi/toplama kinetiğinin iyileştirilmesiyle tutarlıdır. AM1.5G aydınlatması altında ZE-3MeO içeren en yüksek verimli aygıt, açık devre gerilimi (V_{oc}) = 680 mV, kısa devre akım yoğunluğu (J_{sc}) = 12.1 mA/cm², dolum faktörü (FF) = 61.5% ve güç dönüşüm verimi (PCE) = 5.1% değerlerine ulaşırken; modifiye edilmemiş kontrol aygıttan PCE = 4.1% elde edilmiştir. Bu sonuç, yaklaşık %24'lük verim artışına karşılık gelmekte olup, IPCE'den entegre edilen fotoakım değerleriyle uyumludur. Genel olarak, bu sonuçlar, trimetoksi ile ikame edilmiş yardımcı adsorbanların pasivasyonu ve arayüzey yük transferini artırdığını ve DSSC'lerde yeni nesil kendiliğinden organize olan tek tabaka (SAM) benzeri ko-adsorbanlar için tasarım kılavuzu sağladığını göstermektedir.

Anahtar Kelimeler: *Ko-adsorban; SAM; DSSCs; Güneş hücresi; Arayüz modifikasyonu; Verimlilik*

1. Introduction

Dye-sensitized solar cells (DSSCs) continue to garner attention for their low fabrication cost, mechanical compliance, and excellent performance under indoor illumination (Gong *et al.* 2017, Devadiga *et al.* 2021, Muñoz-García *et al.* 2021). In a typical device configuration, photon absorption by the sensitizer is followed by electron injection into the conduction band of the semiconductor (e.g., titanium dioxide, TiO_2), and the redox electrolyte subsequently regenerates the oxidized dye (Brian O'Regan and Michael Gratzel 1991). The kinetics and energetics at the dye/TiO_2/electrolyte interfaces ultimately govern device performance, yet surface defect states, uncontrolled dye aggregation, and suboptimal interfacial charge transfer paths remain key bottlenecks to further efficiency improvements (Gong *et al.* 2017, Muñoz-García *et al.* 2021). One of the most effective strategies to overcome these issues involves the introduction of co-adsorbent molecules, which co-assemble with the dye on the TiO_2 surface (Neale *et al.*

*Sorumlu Yazar/Corresponding Author: Adem MUTLU e-posta/e-mail: adem.mutlu@ege.edu.tr

2005, Li *et al.* 2011, Najm *et al.* 2023). Co-adsorbents mitigate π–π stacking interactions among dye molecules, passivate surface trap states, and promote uniform dye adsorption, leading to reduced recombination and improved open-circuit voltage (V_{oc}) (Neale *et al.* 2005, Lee *et al.* 2012, Matsuyoshi *et al.* 2013, Mazloum-Ardakani and Arazi 2019, Rodrigues *et al.* 2021, Larsson *et al.* 2022). Classical co-adsorbents such as deoxycholic acid (DCA) and chenodeoxycholic acid (CDCA) have been widely employed to control surface coverage and steric hindrance effects (Lee *et al.* 2009, Trilaksana *et al.* 2019, Najm *et al.* 2022). More recently, functionalized aromatic co-adsorbents bearing electron-donating or dipolar groups (e.g., $–NH_2$, $–OCH_3$, –SH, and –CN) have emerged as advanced interfacial modifiers capable of tuning surface energetics and charge-transfer kinetics (Kim *et al.* 2015, Cole and Mayer 2022, Saha and Ganguly 2024). Despite this progress, an important gap remains for methoxy-based co-adsorbents: performance variations are often attributed mainly to the presence of $–OCH_3$ groups, whereas the structure-dependent roles of molecular geometry, adsorption configuration, and surface packing which ultimately govern interfacial resistance and recombination have not yet been systematically resolved across different methoxy-containing scaffolds (Wang *et al.* 2005, Lee *et al.* 2011). Methoxy substituents can modulate surface interactions and local dipoles, potentially affecting adsorption geometry and interfacial energetics. Electron-donating methoxy groups can influence the interfacial energetics and dye packing, which may translate into improved charge injection/collection and reduced recombination depending on the adsorption configuration (Kim *et al.* 2015). These effects collectively lead to improved charge transport, prolonged carrier lifetime, and suppressed recombination, which are essential for high-performance DSSCs (Avilés-Betanzos *et al.* 2023).

This study investigates interfacial engineering of N719-based DSSCs using a trimethoxy-substituted aromatic co-adsorbent, 4-[5'-(3,4,5-trimethoxyphenyl)-2,2'- bithien -5-yl]benzoic acid (ZE-3MeO), a trimethoxy-substituted, π-conjugated aromatic thiophene co-adsorbent anchored by a carboxylic acid group. ZE-3MeO integrates a rigid conjugated backbone with a trimethoxy-substituted aromatic unit, providing a larger and more versatile molecular footprint compared to simple methoxy benzoic acids, demonstrating more effective regulation of co-adsorption and interfacial organization at the TiO2/N719/electrolyte interface. Spectroscopic and electrochemical characterizations (UV–Vis/IPCE, EIS, and XPS) provides converging evidence that ZE-3MeO chemisorbs on TiO_2 via carboxylate anchoring, consistent with interfacial C–O–Ti linkage formation and an increased contribution of oxygenated carbon species. Dark EIS results are consistent with reduced recombination and improved interfacial charge-transfer kinetics while suppressing trap-assisted recombination. In line with these trends, photovoltaic characterization indicates more efficient photocarrier collection and an overall enhancement in device performance compared with reference cells. The key contribution of this work extends beyond a purely incremental change (i.e., introducing $–OCH_3$ into a known co-adsorbent scaffold) and instead establishes an architecture-driven interfacial design concept, wherein the conjugated molecular geometry and packing propensity of a trimethoxy-substituted co-adsorbent govern the balance between interfacial charge transfer and recombination in DSSCs.

2. Materials and Methods

2.1 Materials

Chloroplatinic acid solution (8 wt%, Sigma-Aldrich) served as the platinum (Pt) precursor. Fluorine doped tin oxide coated glass slide (FTO, TEC-15) (Kintec) was used as the conductive substrate. The sensitizer (N719; di-tetrabutylammonium cis-bis (isothiocyanato)-bis (2,2'-bipyridyl-4,4'-dicarboxylato) ruthenium (II)), together with EL-HPE electrolyte and 18NR-AO TiO_2 paste, was obtained from DYESOL.

2.2 Device Fabrication

Devices (active area: 0.49 cm^2) were fabricated on 2.0 cm × 2.5 cm FTO glass. Substrates were cleaned with detergent, ultrasonicated for 20 min each in deionized water, acetone, and isopropyl alcohol, then treated with oxygen plasma for 7 min. A compact TiO_2 layer was deposited by spin coating (2000 rpm, 20 s) and annealed at 460 °C for 1 h. A mesoporous TiO_2 (m-TiO_2) scaffold was subsequently doctor-bladed and annealed at 500 °C for 1 h. After cooling to ~80 °C, films were sensitized for 24 h in 0.5 mM N719 prepared in a 1:1 (v/v) dimethyl sulfoxide (DMSO):ethanol mixture. For ZE-3MeO co-adsorption, the ZE-3MeO stock solution (0.1 mM in DMSO) was added to the dye bath immediately before the sensitization process to adjust the final ZE-3MeO concentration to 0.03 mM (9 µL of stock solution was added to 3 mL of 0.5 mM N719 dye bath). Prior to detailed characterization, the amount of ZE-3MeO was pre-tested by varying the stock volume added to a 3 mL dye bath from 3 to 12 µL, while keeping other fabrication conditions the same; 9 µL provided the best overall photovoltaic response, and therefore all subsequent analyses were performed for 9 µL. Platinum counter electrodes were produced by drop-

casting the Pt precursor onto FTO and annealing at 450 °C for 30 min.

2.3 Characterization

The UV–Vis absorption spectrum of the ZE-3MeO material in the solution phase (in chloroform) was measured with a PerkinElmer Lambda 950 UV–Vis–NIR spectrophotometer. Film thickness (m-TiO_2) was obtained via Ambios P7 stylus profilometer. Surface-sensitive XPS was acquired on a PHI VersaProbe, and spectra were modeled in CasaXPS (v2.3.26PR1.0) using the LA(1,643) line-shape function. For photovoltaic tests, the irradiance was set to 100 mW/cm^2 under an AM1.5G. The light intensity (100 mW/cm^2) was calibrated using a certified 4 cm^2 Si reference cell prior to each measurement. J–V curves were then recorded under forward scan on a solar simulator connected to a Keithley (model 2400). IPCE measurements were obtained with an Enlitech QE-R system. EIS measurements were performed in the dark over the frequency range of 100 mHz to 1 MHz using a Zahner IM6, with a 10 mV AC perturbation applied around the selected DC operating point.

3. Results and Discussions

In N719-sensitized DSSCs, the influence of the ZE-3MeO co-adsorbent on device performance was elucidated through comprehensive characterization. The ZE-3MeO/TiO_2 interface chemistry and surface passivation were investigated using UV-Vis and XPS, while the effects on charge injection/extraction, recombination pathways, and interface resistances were quantitatively determined using J-V and EIS measurements. Instead, electron-donating methoxy substituents are expected to regulate interfacial interactions, thereby regulating charge-transfer and recombination pathways at the TiO_2/dye/electrolyte junction and improving device performance.

To elucidate the co-adsorbent function of ZE-3MeO, its optical response was examined. As depicted in Figure 1a, the UV–Vis spectrum of ZE-3MeO displays a relatively narrow band centered in the near-UV/violet region (~390–410 nm) with only a weak tail extending to 450 nm, and no measurable absorption beyond 450 nm where the N719 dye exhibits a strong metal-to-ligand-charge-transfer (MLCT) band (Bedja and Hagfeldt 2011, Vemula *et al.* 2024). These results indicate that ZE-3MeO lacks the electronic transitions necessary for visible-light harvesting and therefore is not expected to contribute directly to photocurrent generation; rather, it acts at the interface, consistent with reduced surface trapping and regulated interfacial charge-transfer/recombination processes (Najm *et al.* 2020). For reference, the m-TiO_2 film thickness was ~9 µm (Figure 1b).

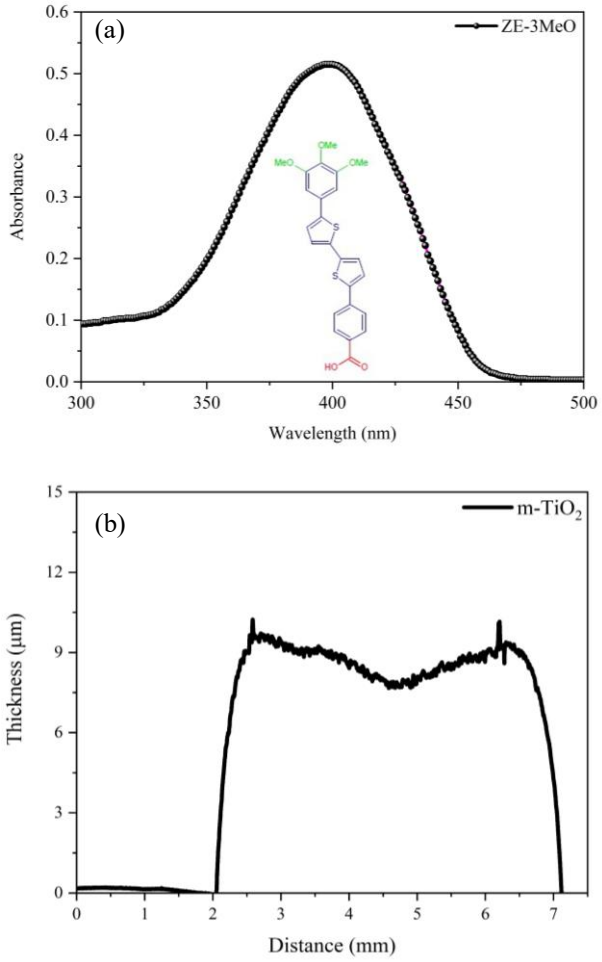

Figure 1. a) UV–Vis absorption spectra of ZE-3MeO in solution phase, b) thickness of the m-TiO_2 layer.

XPS was performed to elucidate the surface chemical environment of the trimethoxy-substituted ZE-3MeO molecule after immobilization onto TiO_2. High-resolution C 1s, S 2p, and O 1s spectra were fitted and the relative peak areas were used to provide comparative metrics (Figure 2; Table 1). In the C 1s spectrum (Figure 2a), the main contribution at 284.27 eV (C–C/C–H) accounts for 57.7% of the total C 1s envelope, representing the aromatic backbone. The oxygenated carbon signals are clearly resolved at 286.04 eV (C–O) and 288.13 eV (O=C–O), contributing 12.6% and 11.74%, respectively. Notably, the C–O component at 286.04 eV is consistent with ether-type C–O–C bonds from methoxy groups and/or surface-associated C–O species, potentially including Ti–O–C-like interactions upon adsorption (Montagne *et al.* 2009, Yameen *et al.* 2010, Choi *et al.* 2013, Easton and Morgan 2025).

In the S 2p region (Figure 2b), the reduced sulfur doublet (S $2p_{3/2}$ at 163.33 eV and S $2p_{1/2}$ at 164.50 eV) contributes 35.45% of the S 2p area, while the oxidized sulfur

component at S $2p_{3/2}$ ≈ 168.52 eV accounts for 64.55% (Hasegawa *et al.* 2015, Guo *et al.* 2021). This indicates partial oxidation during surface functionalization/adsorption steps, while showing that a measurable portion of the reduced sulfur associated with the ZE-3MeO backbone is conserved.

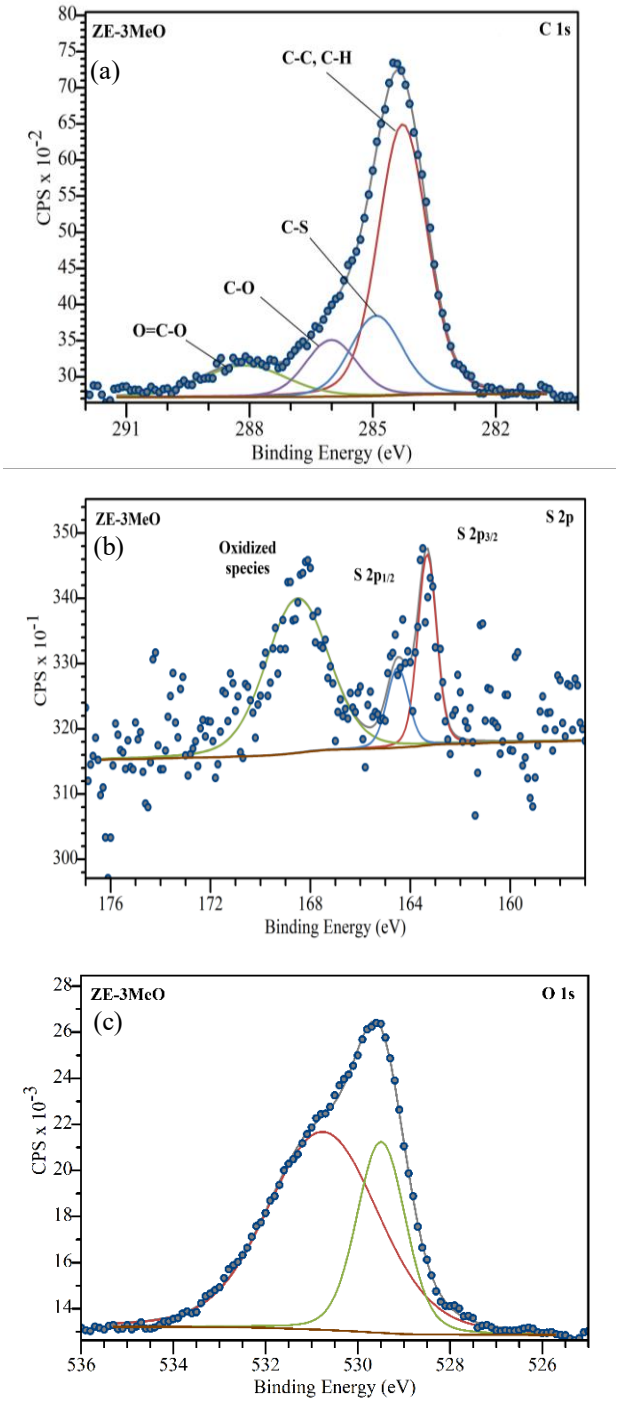

Figure 2. High-resolution XPS spectra of ZE-3MeO molecule on oxide surface: (a) C 1s, (b) S 2p and (c) O 1s spectrum.

Since the peaks associated with the oxidized species are broadened, explicitly resolving their individual contributions increases the risk of overfitting; therefore, they are modeled as a single envelope component to ensure a robust fit and transparent data representation (Yameen *et al.* 2010). The O 1s spectrum (Figure 2c) consists of lattice oxygen from TiO_2 at 529.49 eV (29.83%) and a higher-binding-energy component at 530.76 eV (70.17%). The high-BE O 1s contribution is commonly attributed to surface hydroxyl/chemisorbed oxygen species and/or oxygen in surface-bound organic functionalities, and its magnitude together with the oxygenated fractions in C 1s, is consisted with the presence of ZE-3MeO-derived oxygenated groups at the TiO_2 surface that can contribute to interfacial coordination/anchoring (Zhu *et al.* 2022). Overall, these quantitative area ratios substantiate successful ZE-3MeO immobilization and the formation of an oxygen-rich interfacial chemistry on TiO_2 (Lee *et al.* 2015).

Table 1. Overview of ZE-3MeO binding energies obtained by high-resolution XPS.

	Peaks	BE (eV)	Area	Conc. (%)
O 1s (eV)	O_2^-	529.49	11883.8	29.83
	C=O	530.76	27959.4	70.17
C 1s (eV)	C–C/C–H	284.27	6079.5	57.70
	C–S	284.92	1892.0	17.96
	C–O	286.04	1350.2	12.60
	O=C–O	288.13	1236.9	11.74
S 2p (eV)	2p 3/2	163.33	300.0	23.90
	2p 1/2	164.50	145.0	11.55
	Oxidized species	168.52	810.4	64.55

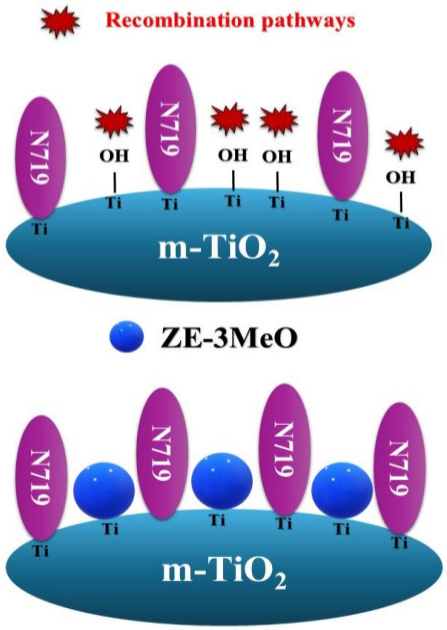

Figure 3. Schematic representation of the ZE-3MeO/m-TiO_2 interface.

These XPS results confirm the successful surface immobilization of ZE-3MeO on TiO_2 and demonstrate its compatibility with trimethoxy-substituted interface chemistry. This interpretation is consistent with the schematic in Figure 3 and shows the proposed

arrangement of ZE-3MeO on the TiO_2 surface. Due to the trimethoxy substitution, ZE-3MeO is expected to form a more ordered and continuous co-adsorbent layer and provide more effective coating of TiO_2 sites. Such an interface arrangement is consistent with enhanced surface passivation, suppressed interface recombination, and improved charge transfer selectivity at the TiO_2/dye/electrolyte interface.

EIS was conducted under dark conditions at the V_{oc} to evaluate the interfacial charge-transfer and recombination characteristics of DSSCs fabricated with and without ZE-3MeO modification (Figure 4) (Wang *et al.* 2005, Öztürk *et al.* 2024, Naik *et al.* 2025). The Nyquist/Bode spectra and fitted parameters reported here were obtained from the highest PCE yielding devices, both with and without ZE-3MeO, fabricated under the optimized protocol. The Nyquist plots exhibited two dominant semicircles, which can be attributed to distinct interfacial processes occurring at different frequency regions. The high-frequency arc is commonly associated with charge transfer at the counter electrode/electrolyte interface, whereas the mid-frequency arc is typically related to charge-transfer/recombination processes at the TiO_2/dye/electrolyte interface. The equivalent circuit used to fit the impedance spectra comprised a series resistance (R_s) and two constant phase element–resistor (CPE–R) pairs, expressed as R_s–(CPE_1/R_1)–(CPE_2/R_2) (Figure 4a inset) (Lazanas and Prodromidis 2023).

The fitted parameters summarized in Table 2 indicate that the ZE-3MeO-modified device exhibits slightly lower series resistance (R_s=17.0 Ω) compared to the control (18.5 Ω), suggesting improved charge transport within the device. R_1 decreased substantially from 6.7 Ω (control) to 3.4 Ω (ZE-3MeO), consistent with facilitated interfacial charge transfer and reduced interfacial losses in the corresponding high-frequency process (Rodrigues *et al.* 2021).

Table 2. Dark-condition EIS parameters for control and ZE-3MeO co-adsorbed DSSCs.

Parameters	Control	ZE-3MeO
R_s (Ω)	18.5	17.0
R_1 (Ω)	6.7	3.4
R_2 (Ω)	7.4	7.5
τ_e (ms)	3.8	16.6

The R_2 remained essentially unchanged (7.4 Ω for the control vs. 7.5 Ω for ZE-3MeO), suggesting that introducing ZE-3MeO does not introduce an additional ohmic loss contribution or reduce the fitted recombination resistance within the sensitivity of the adopted model (Table 2).

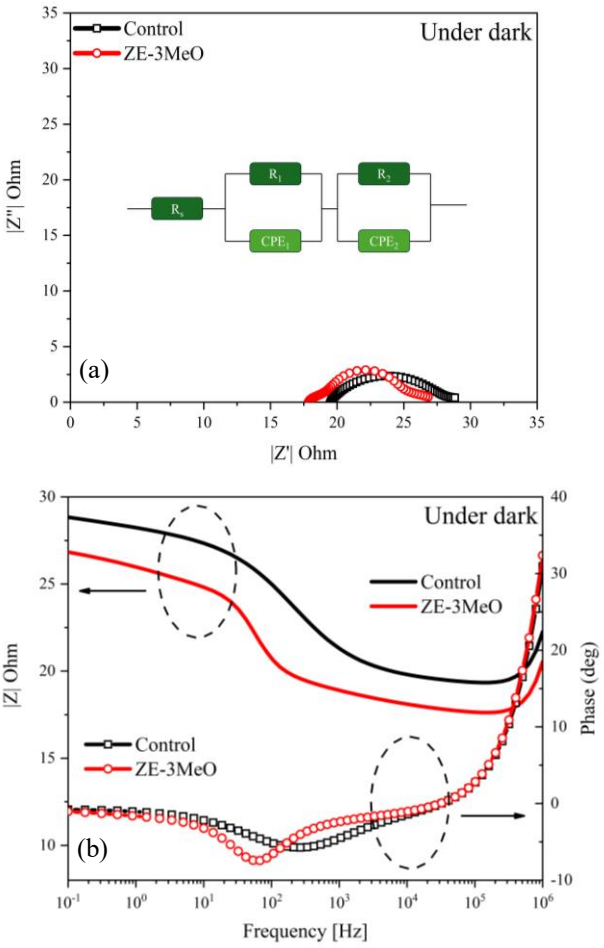

Figure 4. EIS analysis of DSSC devices without and with ZE-3MeO co-adsorbent. (a) Nyquist plots and equivalent circuit, (b) Bode plots.

Notably, despite the near-constant R_2, the electron lifetime (τ_e) extracted from the Bode phase maximum increased markedly from 3.8 ms (control) to 16.6 ms (ZE-3MeO), indicating slower recombination dynamics and/or longer-lived interfacial charge accumulation (Figure 4b) (Cisneros *et al.* 2016). The τ_e was calculated from the Bode phase plots as:

$$\tau_e = \frac{1}{2\pi f_{max}} \quad (1)$$

where f_{max} is the frequency at the maximum phase angle. A shift of the characteristic peak from higher to lower frequency typically indicates a larger time constant, corresponding to a longer electron lifetime for the interfacial process (Weerasinghe *et al.* 2024). These EIS trends support improved interfacial charge-transport/collection behavior and mitigated recombination, in line with the enhanced device performance (Hora *et al.* 2022, Aldosari *et al.* 2023).

As evident from the J–V and IPCE characterizations of the best performing DSSCs fabricated with and without the ZE-3MeO co-adsorbent, the introduction of the trimethoxy-substituted co-adsorbent molecule exerts a

distinct positive effect on photovoltaic performance (Figure 5a). The reference device exhibited a PCE of 4.1 %, whereas the ZE-3MeO-modified device reached a significantly higher efficiency of 5.1 %, primarily attributed to the enhanced J_{sc}=12.1 mA/cm^2 and an improved FF=61.5 % while maintaining a similar V_{oc}=680 mV (Table 3). Although ZE-3MeO improves EIS-derived recombination indicators (e.g., τ_e), V_{oc} remains nearly unchanged. In DSSCs, V_{oc} is governed by the electron quasi-Fermi level in TiO_2 relative to the electrolyte redox potential and thus depends on both recombination kinetics and interfacial energetics (Bisquert and Vikhrenko 2004). Therefore, an interfacial modifier can enhance charge collection (higher J_{sc} and FF) while yielding a limited V_{oc} change if it concurrently induces subtle shifts in the effective TiO_2 conduction-band edge and/or interfacial band alignment (Neale *et al.* 2005b, Lim *et al.* 2011, Sung *et al.* 2020). This improvement indicates that ZE-3MeO effectively facilitates interfacial charge injection and reduces carrier recombination losses at the TiO_2/N719/electrolyte interface (Han *et al.* 2012, Lee *et al.* 2012).

Table 3. Photovoltaic parameters of the champion DSSCs with and without ZE-3MeO co-adsorbent.

ID	J_{sc} (mA/cm^2)$^{J\text{-}V}$	J_{sc} (mA/cm^2)^{IPCE}	V_{oc} (mV)	FF (%)	PCE (%)
Control	10.7	9.4	680	57.7	4.1
ZE-3MeO	12.1	11.2	680	61.5	5.1

Table 4. Averaged J–V characteristics of DSSCs fabricated with and without ZE-3MeO co-adsorbent.

ID	J_{sc} (mA/cm^2)	V_{oc} (mV)	FF (%)	PCE (%)
Control	10.7	680	57.7	4.1
	10.0	680	55.0	3.8
	10.2	675	56.0	3.9
	9.7	675	54.6	3.6
	10.3	670	57.0	4.0
Average	10.18	676	56.06	3.88
ZE-3MeO	12.0	680	60.0	4.9
	12.4	680	58.0	4.9
	12.1	680	61.5	5.1
	11.8	680	61.0	5.0
	11.9	680	61.7	5.0
Average	12.04	680	60.44	4.98

To verify reproducibility, five independent DSSCs were fabricated and measured for each condition following an identical fabrication protocol. The average photovoltaic parameters are summarized in Table 4. The relatively small device-to-device spread in PCE (3.88 ± 0.19% for the control and 4.98 ± 0.08% for ZE-3MeO) confirms good reproducibility and a consistent performance enhancement upon ZE-3MeO modification.

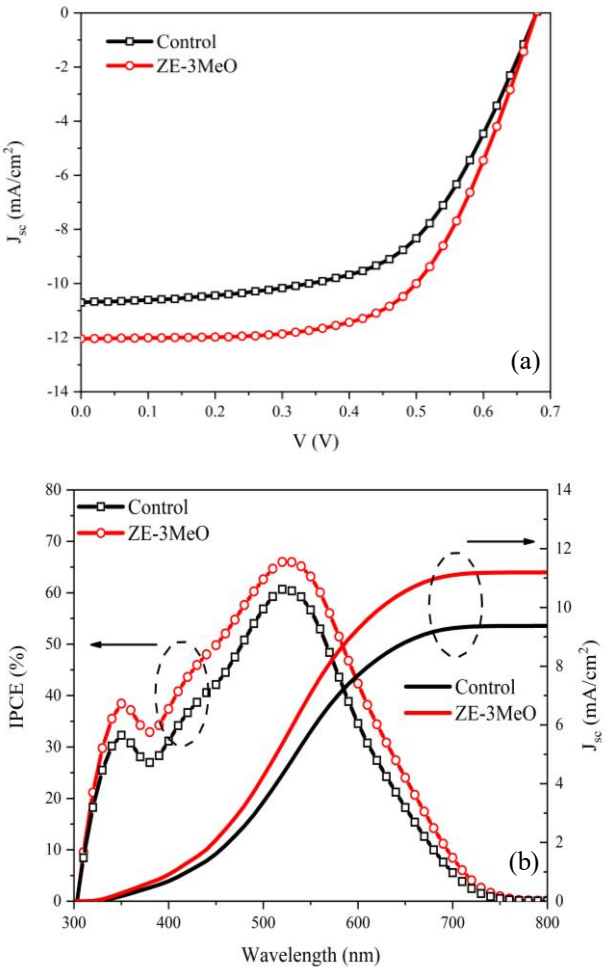

Figure 5. Photovoltaic performance of the champion DSSCs with and without ZE-3MeO co-adsorbent. (a) J–V curves (b) IPCE spectra.

J_{sc} values obtained from both J–V measurements and IPCE integration showed strong consistency, further supporting the reliability of the measured photoresponse (Figure 5b). The IPCE-integrated J_{sc} values were 9.4 mA/cm^2 for the control and 11.2 mA/cm^2 for the ZE-3MeO device, corresponding to a ~7.4% deviation for ZE-3MeO relative to the J–V-derived J_{sc} (12.1 mA/cm^2) and a comparable deviation for the control, which falls within the commonly accepted uncertainty range reported for J_{sc} cross-validation in DSSCs. Such residual discrepancies between J–V and IPCE-derived J_{sc} values can primarily arise from spectral mismatch between the AM 1.5G solar simulator and the monochromatic IPCE setup, as well as temperature-dependent and series-resistance-related effects that are inherently captured during J–V scans but not reflected in IPCE integration. The improved J_{sc} and FF obtained for the ZE-3MeO device are consistent with the dual interfacial role of the trimethoxy-substituted co-adsorbent: (i) strengthening interfacial coupling and facilitating charge transfer/collection, and (ii) mitigating interfacial recombination via surface-state passivation. Consequently, the agreement between the J–V and IPCE

analyses indicates that ZE-3MeO enhances photocurrent generation primarily through improved charge-collection dynamics and interfacial passivation, leading to reproducible performance gains in DSSCs (Chang *et al.* 2013, Zou *et al.* 2022).

To further benchmark our results, we compared our devices with representative reference systems from previous studies (Table 5). ZE-3MeO offers performance that can compete with various basic co-adsorbents and selected interface modifiers. The performance gain observed here is primarily driven by higher J_{sc} and improved FF, whereas the V_{oc} remains comparatively modest an outcome that is broadly consistent with trends reported for trimethoxy-substituted co-adsorbents in N719-based DSSCs. The XPS and EIS signatures are consistent with these performance trends, positioning ZE-3MeO as a practical and scalable co-adsorbent strategy for achieving competitive DSSC performance through improved interfacial regulation.

Table 5. Comparison of photovoltaic parameters for ZE-3MeO-modified N719 DSSCs with benchmark literature.

Co-adsorbent	J_{sc} (mA/cm^2)	V_{oc} (mV)	FF (%)	PCE (%)	Ref.
2-MBT	10.03	719	58.2	4.2	(Larsson *et al.* 2022)
CA	14.87	765	45.7	5.2	(Mazloum-Ardakani and Arazi 2019)
CDCA	8.4	795	55.38	3.69	(Najm *et al.* 2022)
CDCA	14.29	660	67.0	6.31	(Yen *et al.* 2013)
BMPP	>15.0	>750	>70.0	~8.0	(Cisneros *et al.* 2016)
EG0	13.34	734	69.0	6.75	(Xu *et al.* 2013)
mPEG	11.0	760	68.0	5.7	(Lee *et al.* 2012)
TEOS	~9.5	~750	~71.0	4.97	(Lin and Chu 2014)
PTEOS	~9.8	~750	~71.0	5.1	(Lin and Chu, 2014
TBACDC	12.0	803	77.3	7.42	(Neale *et al.* 2005a)
CDCA	12.0	740	72.0	6.4	(Sasitharan *et al.* 2025)
BIAC01L	13.13	760	71.0	7.11	(Sasitharan *et al.* 2025)
BIAC03L	13.1	770	75.0	7.56	(Sasitharan *et al.* 2025)
BIAC05Q	13.1	760	73.0	7.26	(Sasitharan *et al.* 2025)
CDCA	17.44	791	51.0	7.1	(Gnida and Schab-Balcerzak 2024)
CDCA	22.15	720	46.0	7.6	(Gnida and Schab-Balcerzak 2024)
CDCA	24.05	768	46.0	8.5	(Gnida *et al.* 2024)
ZE-3MeO	**12.1**	**680**	**61.5**	**5.1**	**This work**

4. Conclusions

In this study, the interfacial impact of the trimethoxy-substituted co-adsorbent ZE-3MeO on N719-based DSSCs was systematically investigated. The trimethoxy functionalization markedly modifies the surface chemical environment and interfacial charge-transport behavior at the TiO_2/N719/electrolyte interface. XPS indicates enhanced oxygenated-carbon signatures (C–O–C/C–O) and an increased high binding energy O 1s contribution, consistent with an oxygen-enriched interfacial chemistry upon ZE-3MeO adsorption. Dark EIS further supports improved interfacial charge-transfer kinetics, as evidenced by a reduced high-frequency interfacial resistance (R_1 = 3.4 Ω vs 6.7 Ω) and an extended electron lifetime (τ_e = 16.6 ms vs 3.8 ms), consistent with mitigated recombination dynamics. Consistently, the ZE-3MeO-modified device delivers higher J_{sc} (12.1 mA/cm^2) and FF (61.5%), yielding a PCE of 5.1% (vs 4.1%) while maintaining a similar V_{oc} (~680 mV), and the agreement between J–V and IPCE trends corroborates the enhanced charge-collection behavior. Overall, the combined electrochemical, spectroscopic, and photovoltaic results suggest that trimethoxy functionalization mitigates non-radiative losses at the interface, positioning ZE-3MeO as a practical co-adsorbent for interface-engineered DSSCs.

Declaration of Ethical Standards

The authors declare that they comply with all ethical standards.

Credit Authorship Contribution Statement

Author-1: Conceptualization, Methodology, Software, Validation, Formal analysis, Investigation, Resources, Data curation, Writing – original draft, Visualization, Supervision, Project administration, Funding acquisition

Declaration of Competing Interest

The authors have no conflicts of interest to declare regarding the content of this article.

Data Availability Statement

All data generated or analyzed during this study are included in this published article.

Acknowledgment

Support for the XPS analysis was provided by the Scientific and Technological Research Council of Türkiye (TÜBİTAK), Project No. 124F179.

5. References

Aldosari, H., Ali, A., Muqaddas, S., Shoukat, R. and Awad, M.A. 2023. Electrodeposited NiCoO2@CNTs fiber as efficient counter electrode in wire-shaped dye-sensitized solar cells. Journal of Materials Science: Materials in Electronics, 34, 1916. https://doi.org/10.1007/s10854-023-11379-6

Avilés-Betanzos, R., Oskam, G. and Pourjafari, D. 2023. Low-Temperature Fabrication of Flexible Dye-Sensitized Solar Cells: Influence of Electrolyte Solution on Performance under Solar and Indoor Illumination. Energies, 16, 5617. https://doi.org/10.3390/en16155617

Bedja, I. and Hagfeldt, A. 2011. Comparative Study between Dye-Sensitized and CdS Quantum-Dots-Sensitized TiO2 Solar Cells Using Photoinduced Absorption Spectroscopy. Advances in OptoElectronics, 2011, 1–5. https://doi.org/10.1155/2011/424071

Bisquert, J. and Vikhrenko, V.S. 2004. Interpretation of the Time Constants Measured by Kinetic Techniques in Nanostructured Semiconductor Electrodes and Dye-Sensitized Solar Cells. The Journal of Physical Chemistry B, 108, 2313–2322. https://doi.org/10.1021/jp035395y

Brian O'Regan and Michael Gratzel. 1991. A low-cost, high-efficiency solar cell based on dye-sensitized colloidal TiO2 films. Nature 1991; 353; 737–740. https://doi.org/10.1038/353737a0

Chang, S., Wang, H., et al. 2013. Conformational engineering of co-sensitizers to retard back charge transfer for high-efficiency dye-sensitized solar cells. Journal of Materials Chemistry A, 1, 11553. https://doi.org/10.1039/c3ta12714a

Choi, I.T., Ju, M.J., Song, S.H., Kim, S.G., Cho, D.W., Im, C. and Kim, H.K. 2013. Tailor-Made Hole-Conducting Coadsorbents for Highly Efficient Organic Dye-Sensitized Solar Cells. Chemistry – A European Journal, 19, 15545–15555. https://doi.org/10.1002/chem.201301658

Cisneros, R., Beley, M. and Lapicque, F. 2016. A study of the impact of co-adsorbents on DSSC electron transfer processes: anti-π-stacking vs. shield effect. Physical Chemistry Chemical Physics, 18, 9645–9651. https://doi.org/10.1039/C6CP00077K

Cole, J.M. and Mayer, U.F.J. 2022. Characterizing Interfacial Structures of Dye-Sensitized Solar Cell Working Electrodes. Langmuir, 38, 871–890. https://doi.org/10.1021/acs.langmuir.1c02165

Devadiga, D., Selvakumar, M., Shetty, P. and Santosh, M.S. 2021. Dye-Sensitized Solar Cell for Indoor Applications: A Mini-Review. Journal of Electronic Materials, 50, 3187–3206. https://doi.org/10.1007/s11664-021-08854-3

Easton, C.D. and Morgan, D.J. 2025. Critical examination of the use of x-ray photoelectron spectroscopy (XPS) O 1s to characterize oxygen vacancies in catalytic materials and beyond. Journal of Vacuum Science & Technology A, 43, 053205. https://doi.org/10.1116/6.0004686

Gnida, P. and Schab-Balcerzak, E. 2024. Effect of Structural and Material Modifications of Dye-Sensitized Solar Cells on Photovoltaic Performance. Coatings, 14, 837. https://doi.org/10.3390/coatings14070837

Gnida, P., Slodek, A., Łapkowski, M. and Schab-Balcerzak, E. 2024. Impact of DSSCs structure modification sensitized with phenothiazine derivative on photovoltaic performance. Opto-Electronics Review, 152679–152679. https://doi.org/10.24425/opelre.2024.152679

Gong, J., Sumathy, K., Qiao, Q. and Zhou, Z. 2017. Review on dye-sensitized solar cells (DSSCs): Advanced techniques and research trends. Renewable and Sustainable Energy Reviews, 68, 234–246. https://doi.org/10.1016/j.rser.2016.09.097

Guo, D., Li, Z., Liu, P. and Sun, M. 2021. N, P, S co-doped biomass-derived hierarchical porous carbon through simple phosphoric acid-assisted activation for high-performance electrochemical energy storage. International Journal of Hydrogen Energy, 46, 8197–8209. https://doi.org/10.1016/j.ijhydene.2020.12.013

Han, L., Islam, A., et al. 2012. High-efficiency dye-sensitized solar cell with a novel co-adsorbent. Energy & Environmental Science, 5, 6057. https://doi.org/10.1039/c2ee03418b

Hasegawa, G., Deguchi, T., Kanamori, K., Kobayashi, Y., Kageyama, H., Abe, T. and Nakanishi, K. 2015. High-Level Doping of Nitrogen, Phosphorus, and Sulfur into Activated Carbon Monoliths and Their Electrochemical Capacitances. Chemistry of Materials, 27, 4703–4712. https://doi.org/10.1021/acs.chemmater.5b01349

Hora, C., Santos, F., Pereira, A.M.V.M., Sales, M.G.F., Ivanou, D. and Mendes, A. 2022. PEDOT-graphene counter-electrode for solar and improved artificial light conversion in regular, bifacial and FTO-less cobalt mediated DSSCs. Electrochimica Acta, 412, 140140. https://doi.org/10.1016/j.electacta.2022.140140

Kim, S.H., Choi, J., et al. 2015. The effect of the number, position, and shape of methoxy groups in triphenylamine donors on the performance of dye-sensitized solar cells. Dyes and Pigments, 113, 390–401.

https://doi.org/10.1016/j.dyepig.2014.09.014

Larsson, L.F.G., Tractz, G.T., Camargo Matheus, A.P. and Pinto Rodrigues, P.R. 2022. The use of 2-Mercaptobenzothiazole as a new co-adsorbent in dye-sensitized solar cells. Optical Materials, 131, 112658.
https://doi.org/10.1016/j.optmat.2022.112658

Lazanas, A.Ch. and Prodromidis, M.I. 2023. Electrochemical Impedance Spectroscopy–A Tutorial. ACS Measurement Science Au, 3, 162–193.
https://doi.org/10.1021/acsmeasuresciau.2c00070

Lebrun, D., 2010. Thiolsulfinates/Thiolsulfonates formation: X ray photoelectron spectroscopy (XPS) of oxidized thiols on flat surfaces. Master's thesis, Uppsala University, Department of Physics and Astronomy, Materials Physics.

Lee, H.J., Jamison, A.C. and Lee, T.R. 2015. Surface Dipoles: A Growing Body of Evidence Supports Their Impact and Importance. Accounts of Chemical Research, 48, 3007–3015.
https://doi.org/10.1021/acs.accounts.5b00307

Lee, K.E., Gomez, M.A., Regier, T., Hu, Y. and Demopoulos, G.P. 2011. Further Understanding of the Electronic Interactions between N719 Sensitizer and Anatase TiO2 Films: A Combined X-ray Absorption and X-ray Photoelectron Spectroscopic Study. The Journal of Physical Chemistry C, 115, 5692–5707.
https://doi.org/10.1021/jp109869z

Lee, K.-M., Wu, S.-J., et al. 2009. Efficient and stable plastic dye-sensitized solar cells based on a high light-harvesting ruthenium sensitizer. *Journal of Materials Chemistry*, 19, 5009.
https://doi.org/10.1039/b903852c

Lee, Y.-G., Park, S., et al. 2012. Effective Passivation of Nanostructured TiO_2 Interfaces with PEG-Based Oligomeric Coadsorbents To Improve the Performance of Dye-Sensitized Solar Cells. *The Journal of Physical Chemistry C*, 116, 6770–6777.
https://doi.org/10.1021/jp210360n

Li, J., Wu, W., Yang, J., Tang, J., Long, Y. and Hua, J. 2011. Effect of chenodeoxycholic acid (CDCA) additive on phenothiazine dyes sensitized photovoltaic performance. *Science China Chemistry*, 54, 699–706.
https://doi.org/10.1007/s11426-011-4227-9

Lim, J., Kwon, Y.S. and Park, T. 2011. Effect of coadsorbent properties on the photovoltaic performance of dye-sensitized solar cells. *Chemical Communications*, 47, 4147.
https://doi.org/10.1039/c0cc04999a

Lin, C.-L. and Chu, C.-M. 2014. A Study on the Effects of Siloxane Derivatives as Co-adsorbents on the Performance of Dye-sensitized Solar Cells. *Energy Procedia*, 61, 842–845.
https://doi.org/10.1016/j.egypro.2014.11.978

Matsuyoshi, H., Tomita, H., Nishino, H., Sakamoto, H. and Manabe, K. 2013. The Effects of Malonic Acid Derivatives and Acetic Acid Derivatives as Coadsorbents on the Photovoltaic Performance of Dye-Sensitized Solar Cells. *International Journal of Photoenergy*, 2013, 1–6.
https://doi.org/10.1155/2013/439717

Mazloum-Ardakani, M. and Arazi, R. 2019. Improving the effective photovoltaic performance in dye-sensitized solar cells using an azobenzenecarboxylic acid-based system. *Heliyon*, 5, e01444.
https://doi.org/10.1016/j.heliyon.2019.e01444

Montagne, F., Polesel-Maris, J., Pugin, R. and Heinzelmann, H. 2009. Poly(*N* -isopropylacrylamide) Thin Films Densely Grafted onto Gold Surface: Preparation, Characterization, and Dynamic AFM Study of Temperature-Induced Chain Conformational Changes. *Langmuir*, 25, 983–991.
https://doi.org/10.1021/la803729p

Muñoz-García, A.B., Benesperi, I., et al. 2021. Dye-sensitized solar cells strike back. *Chemical Society Reviews*, 50, 12450–12550.
https://doi.org/10.1039/D0CS01336F

Naik, P., Abdellah, I.M., Abdel-Shakour, M., Keremane, K.S. and Adhikari, A.V. 2025. Enhancing the Photoelectrochemical Performance of Ru(II)-Sensitized Dye-Sensitized Solar Cells Using Cyanopyridine-Based Cosensitizers. *Energy Technology*, 2500294.
https://doi.org/10.1002/ente.202500294

Najm, A.S., A. Ludin, N., et al. 2020. Effect of Chenodeoxycholic Acid on the Performance of Dye-sensitized Solar Cells utilizing Pinang Palm (Areca catechu) Dye. *Sains Malaysiana*, 49, 3017–3028.
https://doi.org/10.17576/jsm-2020-4912-13

Najm, A.S., Ahmad Ludin, N., Jaber, I., Hamid, N.H. and Salah Naeem, H. 2022. Influence of the concentration of chenodeoxycholic acid on the performance of the N719 dye. *Inorganica Chimica Acta*, 533, 120776.
https://doi.org/10.1016/j.ica.2021.120776

Najm, A.S., Alwash, S.A., Sulaiman, N.H., Chowdhury, M.S. and Techato, K. 2023. N719 dye as a sensitizer for dye-sensitized solar cells (DSSCs): A review of its functions and certain rudimentary principles. *Environmental Progress & Sustainable Energy*, 42, e13955.
https://doi.org/10.1002/ep.13955

Neale, N.R., Kopidakis, N., Van De Lagemaat, J., Grätzel, M. and Frank, A.J. 2005b. Effect of a Coadsorbent on the Performance of Dye-Sensitized TiO2 Solar Cells: Shielding versus Band-Edge Movement. The Journal of Physical Chemistry B, 109, 23183–23189.
https://doi.org/10.1021/jp0538666

Öztürk, N., Bekmez, M.G., Arslan, B.S., Bulut, E., Avcı, D., Şişman, İ. and Nebioğlu, M. 2024. Acridine-based metal-free organic dyes with various auxiliary acceptors for dye-sensitized solar cells. Dyes and Pigments, 225, 112061. https://doi.org/10.1016/j.dyepig.2024.112061

Rodrigues, D.F.S.L., Santos, F., Abreu, C.M.R., Coelho, J.F.J., Serra, A.C., Ivanou, D. and Mendes, A. 2021. Passivation of the TiO2 Surface and Promotion of N719 Dye Anchoring with Poly(4-vinylpyridine) for Efficient and Stable Dye-Sensitized Solar Cells. ACS Sustainable Chemistry & Engineering, 9, 5981–5990. https://doi.org/10.1021/acssuschemeng.1c00842

Saha, A. and Ganguly, B. 2024. Exploiting the role of coadsorbents on photovoltaic performances of dye sensitized solar cells: A DFT study. Journal of Molecular Graphics and Modelling, 127, 108678. https://doi.org/10.1016/j.jmgm.2023.108678

Sasitharan, K., Mora Abarca, A.J., Cucinotta, F., Pineda, L.W., Soto Tellini, V.H. and Freitag, M. 2025. Bile acid derivatives as novel co-adsorbents for enhanced performance of blue dye-sensitized solar cells. Communications Chemistry, 8, 75. https://doi.org/10.1038/s42004-025-01433-1

Sung, H.K., Lee, Y., Kim, W.H., Lee, S.-J., Sung, S.-J., Kim, D.-H. and Han, Y.S. 2020. Enhanced Power Conversion Efficiency of Dye-Sensitized Solar Cells by Band Edge Shift of TiO2 Photoanode. Molecules, 25, 1502. https://doi.org/10.3390/molecules25071502

Trilaksana, H., Shearer, C., Kloo, L. and Andersson, G.G. 2019. Restructuring of Dye Layers in Dye Sensitized Solar Cells: Cooperative Adsorption of N719 and Chenodeoxycholic Acid on Titania. ACS Applied Energy Materials, 2, 124–130. https://doi.org/10.1021/acsaem.8b01864

Vemula, S.K., Chelli, S.M., Biswas, C., Soma, V.R. and Raavi, S.S.K. 2024. Adsorption and electron injection studies in N719 sensitized Ag − , Au − implanted and O2 annealed titania films. Optical Materials, 154, 115633. https://doi.org/10.1016/j.optmat.2024.115633

Wang, Q., Moser, J.-E. and Grätzel, M. 2005. Electrochemical Impedance Spectroscopic Analysis of Dye-Sensitized Solar Cells. The Journal of Physical Chemistry B, 109, 14945–14953. https://doi.org/10.1021/jp052768h

Weerasinghe, M.I.U., Kumarage, P.M.L., et al. 2024. Active carbon derived from rice husk as sustainable substitutes for costly platinum electrodes in dye-sensitized solar cells. Journal of Science: Advanced Materials and Devices, 9, 100749. https://doi.org/10.1016/j.jsamd.2024.100749

Xu, J., Wu, H., Jia, X., Kafafy, H. and Zou, D. 2013. Amidoamine dendron-based co-adsorbents: improved performance in dye-sensitized solar cells. Journal of Materials Chemistry A, 1, 14524. https://doi.org/10.1039/c3ta12817b

Yameen, B., Ali, M., Álvarez, M., Neumann, R., Ensinger, W., Knoll, W. and Azzaroni, O. 2010. A facile route for the preparation of azide-terminated polymers. “Clicking” polyelectrolyte brushes on planar surfaces and nanochannels. Polym. Chem., 1, 183–192. https://doi.org/10.1039/B9PY00201D

Yen, Y.-S., Lin, T.-Y., Hsu, C.-Y., Chen, Y.-C., Chou, H.-H., Tsai, C. and Lin, J.T. 2013. A remarkable enhancement of efficiency by co-adsorption with CDCA on the bithiazole-based dye-sensitized solar cells. Organic Electronics, 14, 2546–2554. https://doi.org/10.1016/j.orgel.2013.06.026

Zhu, T., Olthof, S. and Pauporté, Th. 2022. Titanium dioxide surface energy levels tuning by self-assembled monolayers. Applied Physics Letters, 121, 141602. https://doi.org/10.1063/5.0107202

Zou, J., Tang, Y., et al. 2022. Porphyrins containing a tetraphenylethylene-substituted phenothiazine donor for fabricating efficient dye sensitized solar cells with high photovoltages. Journal of Materials Chemistry A, 10, 1320–1328. https://doi.org/10.1039/D1TA09415G